SCIENCE CHINA
Physics, Mechanics & Astronomy

Dewetting in associating lattice gas model confined by hydrophobic walls

Tássylla O. Fonseca, Marcia M. Szortyka, Patrícia Ternes, Cristina Gavazzoni, Alan B. de Oliveira and Marcia C. Barbosa

Citation: SCIENCE CHINA Physics, Mechanics & Astronomy **62**, 107009 (2019); doi: 10.1007/s11433-019-9416-3

View online: http://engine.scichina.com/doi/10.1007/s11433-019-9416-3

View Table of Contents: http://engine.scichina.com/publisher/scp/journal/SCPMA/62/10

Published by the Science China Press

Articles you may be interested in

PREDICTION OF CONFINED TURBULENT GAS-PARTICLE JETS BY AN ENERGY EQUATION MODEL OF PARTICLE TURBULENCE
Science in China Series A-Mathematics, Physics, Astronomy & Technological Science **33**, 52 (1990);

Dense gas-particle flow in vertical channel by multi-lattice trajectory model
SCIENCE CHINA Technological Sciences **55**, 542 (2012);

LATTICE GAS SIMULATION OF VISCOUS FLOW IN A CAVITY
Science in China Series A-Mathematics, Physics, Astronomy & Technological Science **33**, 1072 (1990);

Orbital magnetization of the electron gas on a two-dimensional kagomé lattice under a perpendicular magnetic field
SCIENCE CHINA Physics, Mechanics & Astronomy **55**, 1791 (2012);

Implementing a topological quantum model using a cavity lattice
SCIENCE CHINA Physics, Mechanics & Astronomy **55**, 1549 (2012);

SCIENCE CHINA
Physics, Mechanics & Astronomy

SCIENCE CHINA
Physics, Mechanics & Astronomy

• Article •
Special topic: New advances in water and water systems

October 2019 Vol. 62 No. 10: 107009
https://doi.org/10.1007/s11433-019-9416-3

Dewetting in associating lattice gas model confined by hydrophobic walls

Tássylla O. Fonseca[1*], Marcia M. Szortyka[2*], Patrícia Ternes[3], Cristina Gavazzoni[4], Alan B. de Oliveira[5], and Marcia C. Barbosa[1*]

[1]*Instituto de Fśica, Universidade Federal do Rio Grande do Sul, Porto Alegre 91501-970, Brasil;*
[2]*Universidade Federal de Santa Catarina, Rua Pedro João Pereira, Mato Alto 88900-000, Brasil;*
[3] *Instituto Federal Catarinense, São Bento do Sul 89283-064, Brasil;*
[4] *Instituto de Química, Universidade Estadual de Campinas, Campinas 13083-970, Brasil;*
[5]*Departamento de Física ,Universidade Federal de Ouro Preto, Ouro Preto 35400-000, Brasil*

Received January 10, 2019; accepted April 23, 2019; published online May 27, 2019

The phase behavior of a two dimensional fluid confined within hydrophobic walls is obtained by Monte Carlo simulations. The fluid is described by the associating lattice gas model which reproduces the density and diffusion anomalous behavior of water. The confined fluid exhibits a liquid-liquid critical temperature which decreases with the decrease of the distance between the confining walls. In contact with the wall a dewetting is observed. The thickness of this interfacial layer is independent of the distance between the two walls. Even for very small distances between the two walls no total depletion is observed and consequently no drying transition is present.

water, lattice, confined

PACS number(s): 47.55.nb, 47.20.Ky, 47.11.Fg

Citation: T. O. Fonseca, M. M. Szortyka, P. Ternes, C. Gavazzoni, A. B. de Oliveira, and M. C. Barbosa, Dewetting in associating lattice gas model confined by hydrophobic walls, Sci. China-Phys. Mech. Astron. **62**, 107009 (2019), https://doi.org/10.1007/s11433-019-9416-3

1 Introduction

Nanoconfined geometries containing water are common in nature [1-7] and have been employed to increase the mobility of water [8-11] and to avoid crystallization [12-15]. Understanding the thermodynamic and dynamic of water under these extreme conditions, allow us to explore not only as tools to manipulate natural phenomena but also as scientific strategies to understand the behavior of bulk water.

Usually the confinement introduces two new factors not present in the bulk: an interaction between the fluid and the wall particles and a geometrical limitation which can affect the organization of the particles. For water in contact with an hydrophobic surface the first factor dominates. In this case the repulsive interaction between the surface and the fluid creates a low density contact layer in coexistence with the bulk liquid at a certain distances from the wall [16]. The crossover from this low density layer to the bulk density in the case of water at ambient temperature can be evaluated to be of order of one nanometer [17]. This surface low density water layer were observed both in experiments [18-20] and in simulations [20]. Then it becomes natural to think that as two

*Corresponding authors (Tássylla O. Fonseca, email: tassyllaoliveirafons@gmail.com; Marcia M. Szortyka, email: marcia.szortyka@ufsc.br; Marcia C. Barbosa, email: marcia.barbosa@ufrgs.br)

© Science China Press and Springer-Verlag GmbH Germany, part of Springer Nature 2019
Downloaded to IP: 192.168.0.24 On: 2019-05-28 09:08:46 http://engine.scichina.com/doi/10.1007/s11433-019-9416-3

hydrophobic surfaces approach, the dewetting surface overlaps creating a imbalance in pressure between the bulk water outside the plates and the dewetting region between them causing the two surfaces to attract [21]. This drying transition was observed in simulations [21-24] for water confined between finite and perfect plates and finite polymers in water [25].

Is this mechanism of attraction between hydrophobic surfaces universal? Can we define a particular type of system in which the drying transition should be present? The answers to these questions are still under debate. Simulations in small peptides show the drying first order transition in the protein nanoscale channels [26, 27], particularly if long range electrostatic forces are not present. However studies with protein folding show no sign of dewetting transition as the groups in the protein collapse [28]. When the electrostatic protein-water forces are turned off, a dewetting transition in the interdomain occurs. Similarly association of polyalamine and polyleucine α-helix show no dewetting transition between the chains [29]. In these last two systems [28, 29], the water is not confined in a channel but at the biomolecule surfaces. Consistent with this observation for biomolecules, first principles molecular dynamic simulations show that water confined in single wall long carbon nanotubes and large graphene sheets show that the surface induces density fluctuations with a small layer of dewetting. The size and structure of this layer do not depend on the distance between the confining geometry and no drying transition was observed in simulations [30] and in experiments [31-33] for similar structures.

Berne and collaborators [26] attempted to reconcile the idea that when two hydrophobic structures approach, a drying transition emerges, with the absence of this transition in a number of large biomolecules. In particular they showed that the drying transition observed in melittin tetramer is suppressed when mutations of three hydrophobic isoleucine residues are introduced. Consistent to the Berne and collaborators' [26] studies, prior studies of Huang and collaborators [22] showed that the drying seen between hydrophobic surfaces is suppressed when attractive interactions between the surface and water are incorporated.

A comparison between water behavior at biomolecules and rigid confining geometries suggests that water at small confining geometries and small biomolecules lead the collapse or drying transition in the solute while water at larger biomolecules and infinite confining systems do not induce the transition.

In this work we partially test this idea. We analyze if the assumption that water confined in purely repulsive walls shows a drying transition as the two walls approach. Our analysis avoids any additional interactions due to geometry, combination of attractive and repulsive groups which can add complexity to the problem [30] by employing a very simple water-like fluid, the Associated Lattice Gas Model [34-36]. We adopt this model due to its simplicity and because it reproduces the density and the diffusion anomalous behavior of water [34-36]. In addition of testing if a drying transition appears, we also check if the confinement introduces the shift in the bulk liquid-gas, liquid-liquid and melting transitions as observed in confined fluids [23, 24, 37, 38]. We call dewetting layer when the system form a layer of gas-like structure close to the wall and drying transition if this dewetting layer grows forming one gas phase between the interfaces creating an attractive force between them.

2 Model and methods

We consider the associating lattice gas model in a triangular lattice as introduced by Henriques and collaborators [34, 36]. This two dimensional fluid is confined in a lattice with size L_x and L_y where periodic boundary conditions are applied at the dimension L_y while L_x is finite to reproduce the confinement of the system. The fluid particle is represented by an occupational variable, σ_i, which assumes the value $\sigma_i = 0$, if the site is empty, or $\sigma_i = 1$, if the site is full. In order to represent the orientational degrees of freedom present, for instance, in water, each particle also has additionally six "arms", $\tau_i{}^A$, that represent the different orientations that a particle might exhibit as illustrated by the Figure 1.

Arm variable can assume the following values: (a) $\tau_i^A = 1$ which can represent in the case of water the electron donor (charge distribution at the oxygen vicinity), (b) $\tau_i^A = -1$ which can represent in the case of water the electron acceptor (charge distribution at the hydrogen vicinity) and $\tau_i{}^A = 0$ which represent non bonding directions. In order to represent the tetrahedral structure of water, each particle has two acceptor, two donor and two opposite inert arms as illustrated in Figure 2. Therefore each particle can be in one of eighteen configurational states as indicated by Figure 3. A bond, in the case of water a hydrogen bond, is formed when two neighboring sites have arms with complementary orientations,

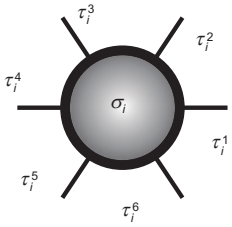

Figure 1 Schematic representation of a particle of the lattice with its occupational, σ_i, and orientational variables, $\tau_i{}^A$, where its six arms are presented, $A = 1, 2, 3, \cdots, 6$.

Downloaded to IP: 192.168.0.24 On: 2019-05-28 09:08:46 http://engine.scichina.com/doi/10.1007/s11433-019-9416-3

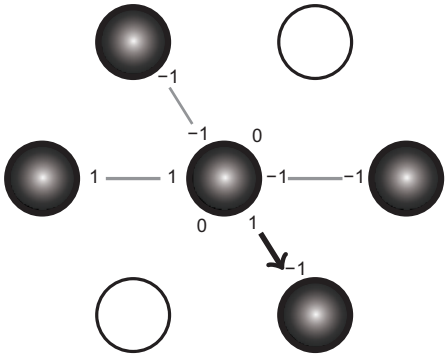

Figure 2 Representation of the central particle, site i, with its six arms and its six first neighbors, sites j, with arms pointing to it. Solid gray lines represent a non-binding configuration, while the arrow represents a binding configuration. We can observe the formation of a hydrogen bond, represented by the arrow, that leaves the central particle (donor arm) and points to its neighbor (acceptor arm).

${\tau_i}^A{\tau_i}^B = -1$, that is, the product of the arms is equal to -1 if a donor arm points to a acceptor arm.

The fluid is then confined between two lines of fixed particle as represented in Figure 4. Here we explore only non interacting walls. The idea is to test if finite system show new phases in addition to the shift of the bulk properties. The energy of the fluid is obtained by separating the sites in two cases: the sites belonging to the central layers and the sites at the contact with the wall layer. Therefore, particles at the central layers are described by the Hamiltonian

$$\hat{\mathcal{H}}_{\text{central}} = (-v + 2u)\sum_{\langle i,k\rangle}^{*}\sigma_i\sigma_k + u\sum_{\langle i,k\rangle}^{*}\sigma_i\sigma_k\sum_{A=1}^{6}\sum_{B^*=1}^{6}\left[\left(1-\tau_i^A\tau_k^B\right)\tau_i^A\tau_k^B\right], \quad (1)$$

where the fluid-fluid interaction is over the six first neighbors, while particles at the contact layer are described by the Hamiltonian

$$\hat{\mathcal{H}}_{\text{contact}} = (-v + 2u)\sum_{\langle i,k\rangle}^{*}\sigma_i\sigma_k + u\sum_{\langle i,k\rangle}^{*}\sigma_i\sigma_k\sum_{A=1}^{4}\sum_{B^*=1}^{4}\left[\left(1-\tau_i^A\tau_k^B\right)\tau_i^A\tau_k^B\right], \quad (2)$$

where the fluid-fluid interaction is over four neighbors since two first neighbors in this case are non interacting particle walls. In these Hamiltonians, $\sigma_i = 0, 1$ are occupation variables, ${\tau_i}^A$ and $\tau_i^{\text{B}} \pm 1$ represent the arm state variables.

For $u/v > 1/2$ the nonbonding first neighbors show a repulsive interaction, $2u - v$, while bonding first neighbors exhibit an attractive energy of $-v$. Since we want to understand the behavior of bonding liquids under confinement, here we employ $u/v = 1$. Throughout our analysis we employ temperature and chemical potential in reduced units

$$\overline{T} = \frac{k_B T}{v}, \quad (3)$$

$$\overline{\mu} = \frac{\mu}{v}. \quad (4)$$

The model properties for the bulk and confined systems were obtained through Monte Carlo simulations using the Metropolis algorithm. Particle insertion and exclusion were tested in the grand canonical ensemble. Data production was generated at fixed chemical potential.

At low chemical potential the initial configuration employed was the empty lattice while for high chemical potential, the lattice was full. Difference initial configurations were tested with no difference in the final structure and density. For both bulk and confined system the direction with periodic conditions was tested for $L_y = 10$, 20, 30 and 50. Results for the density of the confined system for $L_y = 50$ are very similar to the case $L_y = 30$, therefore all the data presented here is for this size. We performed simulations for the confined

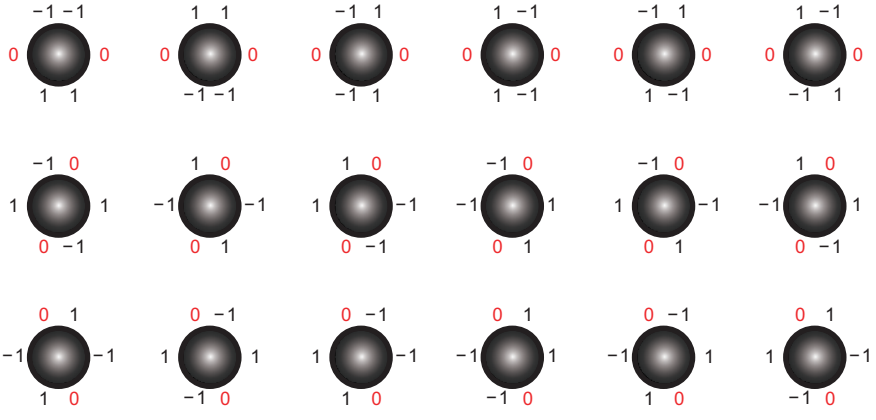

Figure 3 (Color online) Directions of the inert arms (these are diagonally opposite).

Downloaded to IP: 192.168.0.24 On: 2019-05-28 09:08:46 http://engine.scichina.com/doi/10.1007/s11433-019-9416-3

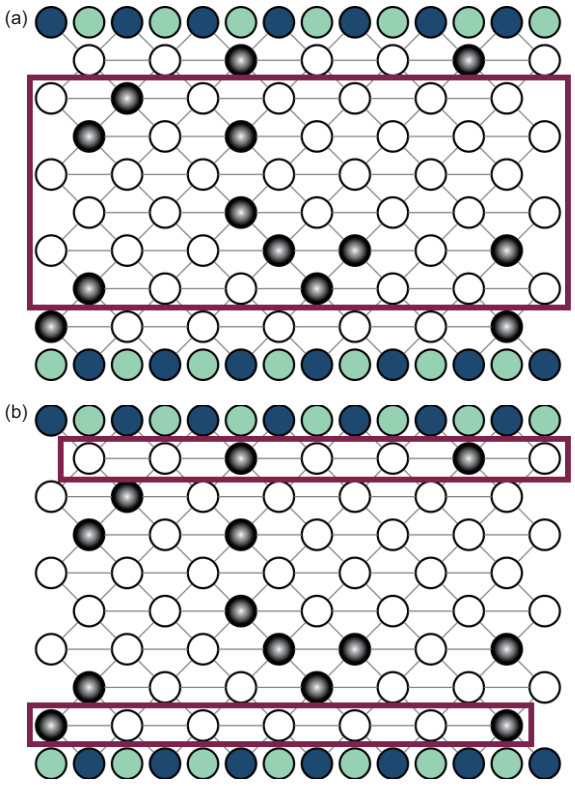

Figure 4 (Color online) Schematic representation highlighting the two regions of the confined system. (a) Sites of the central layers and (b) sites belonging to the layers in contact with the confining walls. The light and dark green circles represent the wall, the filled black circles represent the water particles and the white circles represent the empty sites.

direction $L_x = 2, 4, 6, 8, 10, 60$ and 100. Even thought for $L_x = 60$ and 100 no periodic boundary conditions were employed, the density versus chemical potential for a fixed temperature showed a profile very similar to the bulk behavior but with a dewetting layer still present (we will return to this point later). For equilibration, 2×10^7 Monte Carlo steps were required. The decorrelation time between measurements was 3×10^2 steps from Monte Carlo. Sampling was composed of 5×10^3 measurements.

3 Results

Inspection of the model in the bulk shows at zero temperature three distinct phases. At low chemical potentials, the system is empty and $\rho = 0$. At $\mu^* = -2$ this gas phase coexists with the low density (LDL) liquid phase characterized by an energy per site $e_{\text{gas-LDL}} = E_{\text{gas-LDL}}/L^2 = -3v/2$ and a density $\rho = 0.75$ as illustrated by Figure 5. In the LDL each particle form four bonds with first neighbors. If the chemical potential is further increased, at $\mu^* = -6 + 8u/v$, LDL coexists with the high density (HDL) liquid phase characterized by an energy per site $E_{\text{LDL-HDL}}/L^2 = e_{\text{LDL-HDL}} = -3v + 2u$ and density $\rho = 1$ as illustrated by Figure 5.

In terms of water analogy this simple model can be interpreted as a two length scales interaction potential between particle fluids as follows. Particles at the low density have an average distance of $\bar{d}_{\text{LDL}} = \rho^{1/2} = 2/3^{1/2}$ with average energy per pair of particles of $ep_{\text{LDL}} = E_{\text{LDL}}/\rho_{\text{LDL}} = -v$ while at the high density particles have a distance of $\bar{d}_{\text{HDL}} = \rho^{1/2} = 1$ with energy per pair of particles of $ep_{\text{HDL}} = E_{\text{HDL}}/\rho_{\text{HDL}} = -v + 2u/3$ as illustrated in the Figure 6 for the case $u = v = 1$. The lattice gives the hard core. In the case of water the two length scales represents the interaction between two neighbor particles which can form hydrogen bond (larger distance) or not (closest distance).

This two length scales potential describes a fluid where for a fixed pressure the density increases as the temperature increases and it shows a maximum [34-36], the temperature of maximum density. In addition this simple fluid also has a region in temperatures where the diffusion increases with the

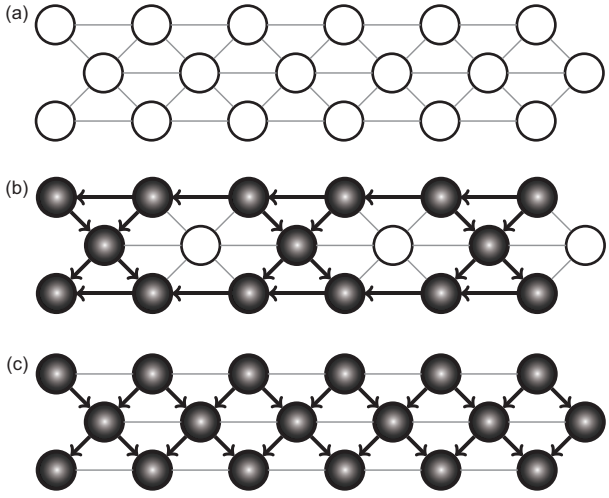

Figure 5 (a) In the gas phase, the whole lattice is empty. (b) In the low density phase, LDL, the lattice is 3/4 filled and particles are distributed over the lattice in such a way that the inert arms point only to the empty sites. There is no energy punishment, in this case. (c) In the high density phase, HDL, the lattice is full, and an energy punishment arises, because two inert arms point to filled sites.

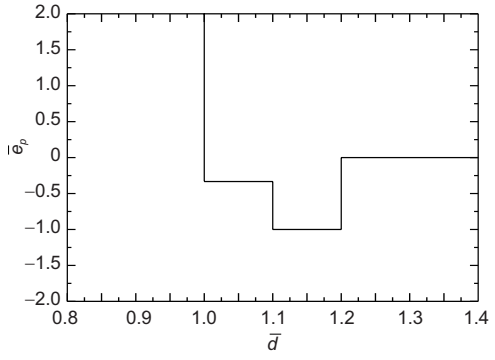

Figure 6 Effective pair potential for the Associated Lattice Gas Model.

Downloaded to IP: 192.168.0.24 On: 2019-05-28 09:08:46 http://engine.scichina.com/doi/10.1007/s11433-019-9416-3

increase of density with a maximum [34]. Both the density and diffusion anomalous behavior are characteristics of water [35] what suggests that the two length scales present in this simple model is able to capture part of the mechanism behind this set of anomalies. The model properties in the bulk for finite temperatures are depicted in the Figure 7 [36]. In addition to the region of density and diffusion anomalies, the system shows a coexistence between the liquid-gas and liquid-liquid phases ending in criticality. The two coexistence lines are jointed by two critical lines. This simple model shows the two liquid phase expected for liquid water. The additional critical lines are an artifact of the symmetry imposed by the lattice.

For the bulk the system exhibits mobility [36], non zero diffusion for a wide range of low temperatures and therefore, the LDL and HDL are considered to be liquid phases. The same terminology will be employed for the confined system.

In principle by confining the system, entropic effects become relevant and a shift of the liquid-gas and liquid-liquid critical temperatures would be expected. Here we explore if this is the case and if the dewetting layer is form and it gives rise to a drying transition as the plates approach.

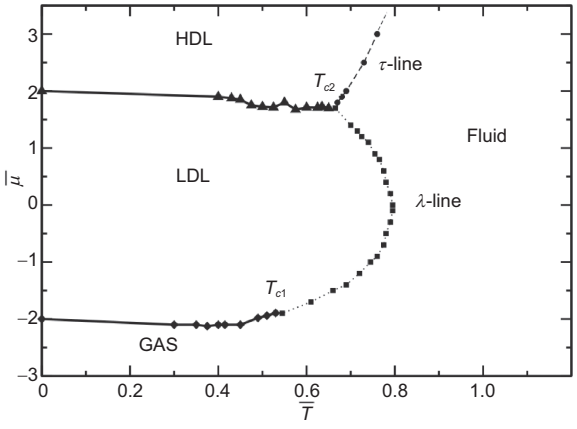

Figure 7 Reduced chemical Potential versus reduced temperature phase diagram for the bulk Associating Lattice Gas Model. Reproduced from ref. [36], with the permission of AIP Publishing.

First, we analyzed the system with two layers of particles, $L_x = 2$. For all temperatures, $\overline{T} = 0.35$ and 0.6, as shown in the Figure 8 not only no phase transition is observed but also the LDL structure is not formed. Therefore, extreme confinement not only suppresses the phase transition but also causes the low-density liquid phase to disappear and causes the gas phase to persist for higher chemical potentials. We did not observe a drying transition but a smooth change from low density to high density layer as the chemical potential is increased.

In order to observe it, by increasing the number of layers of particles, we gradually recover the behavior of the unconfined system, we analyzed the case with four lines of confined sites, that is, $L_x = 4$. The density versus reduced chemical potential illustrated in Figure 9 shows the presence of the ρ= 0.75, the LDL observed in the bulk. For low temperatures, the system exhibits hysteresis between the LDL and HDL phases, characterizing a first order transition. The transition hysteresis becomes narrower as the temperature increases, and the first-order transition between phases gives rise to a critical point.

No phase transition between gas and LDL phases is observed, but a continuous transformation between these two structures indicating that the confinement suppresses this transition. For this confinement at chemical potentials between $\overline{\mu} = -1$ and $\overline{\mu} = 1$ a new structure appears. Figure 10 shows for $\overline{\mu} = 0.875$ and $\overline{T} = 0.35$ this arrangement in which no particle is present at the contact layer. Since this structure dewets from the wall, we call it a Low Hydration Liquid (LHL) phase. This LHL represents the dewetting observed in surfaces as discussed in sect. 1.

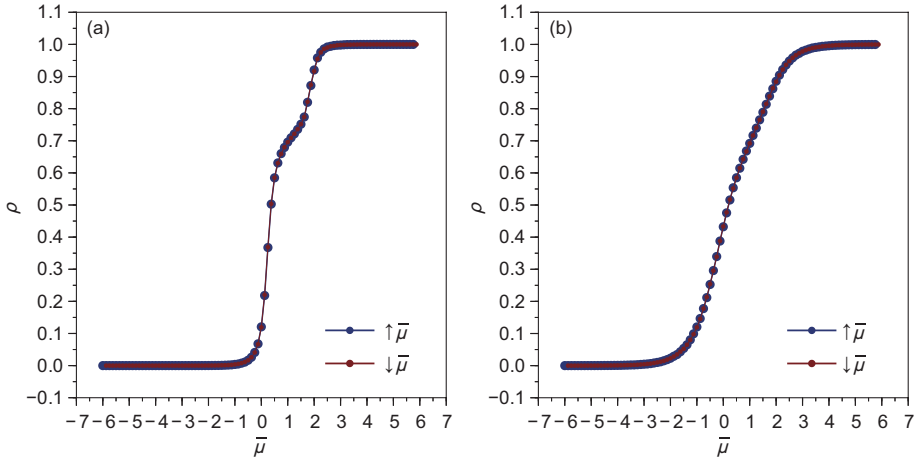

Figure 8 (Color online) Density vs. reduced chemical potential for $L_x = 2$. (a) $\overline{T}$= 0.35 and (b) $\overline{T}$= 0.60.

Downloaded to IP: 192.168.0.24 On: 2019-05-28 09:08:46 http://engine.scichina.com/doi/10.1007/s11433-019-9416-3

The existence of a gas layer in contact to the interface was observed before for simulations inside nanotubes [39] for a fixed temperature and pressure. In our case, we observed this layer emerging and disappearing due to a change in temperature and chemical potential.

In order to verify if this new structure is not an artifact but is present for other confining structure, we study also the L_x= 6, 8 and 10 systems. Figure 11 shows for a fixed temperature $\overline{T}$ = 0.35 that as L_x is increased, the hysteresis between the LHL-LDL becomes wider. Figure 12 illustrates for the same sizes that as the temperature increases the coexistence between the two liquids gives rise to criticality and that as the size increases the critical temperature increases. This result confirms our idea that one important effect of this hydrophobic confinement is the shift of the critical temperature to lower values. As L_x increases the critical temperature of the confined system should approach the critical temperature for the bulk system. In the case of L_x = 10, the jump in the density at $\overline{\mu}$ = −2 indicates the gas-LHL first order transition.

Figure 13 illustrates the dewetting for the L_x = 10 system, showing that the LHL is present even in the largest simulated size. As L_x increases the difference in density between the LHL and LDL decreases, however this occurs because the dewetting layer is only one layer without particles at each wall and as the distance between the wall increases, the impact in the overall density decreases. In order to confirm that no drying phase transition occurs as the two walls are approached, the computed the density excluding the contact layer at the region of chemical potentials, $\overline{\mu} \approx -1$ for which the dewetting layer is present. We observe that the density is

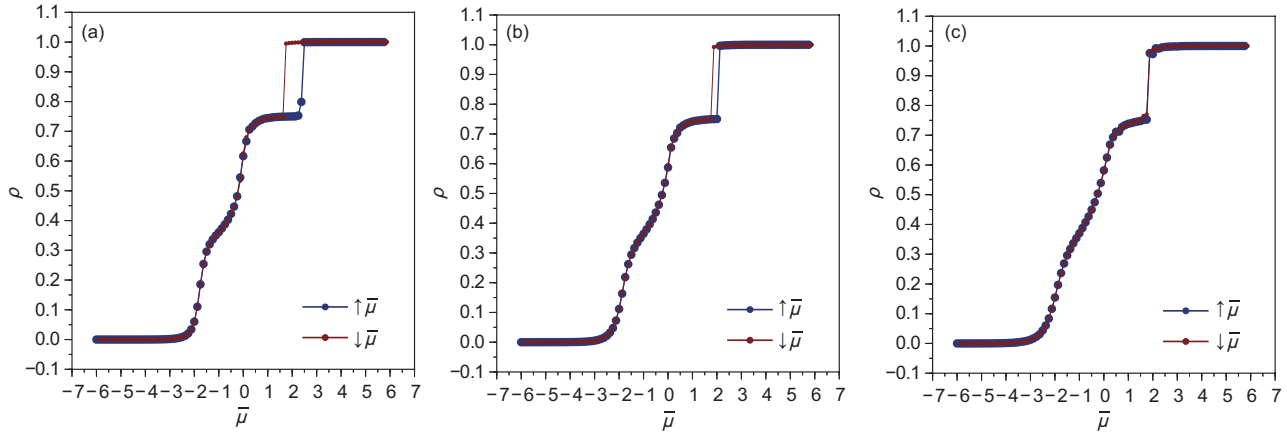

Figure 9 (Color online) Density vs. reduced chemical potential for L_x = 4. (a) $\overline{T}$= 0.35, (b) $\overline{T}$= 0.40 and (c) $\overline{T}$= 0.45.

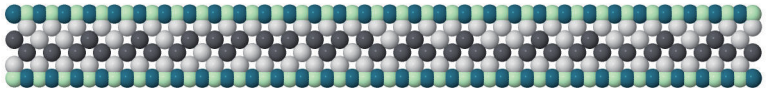

Figure 10 (Color online) Snapshot of the simulation of the confined lattice L_x = 4 in the *x*-*y* plane at $\overline{T}$= 0.35 and $\overline{\mu}$= 0.875. The light and dark green circles represent the wall, the filled black circles represent the water particles and the gray circles represent the empty sites.

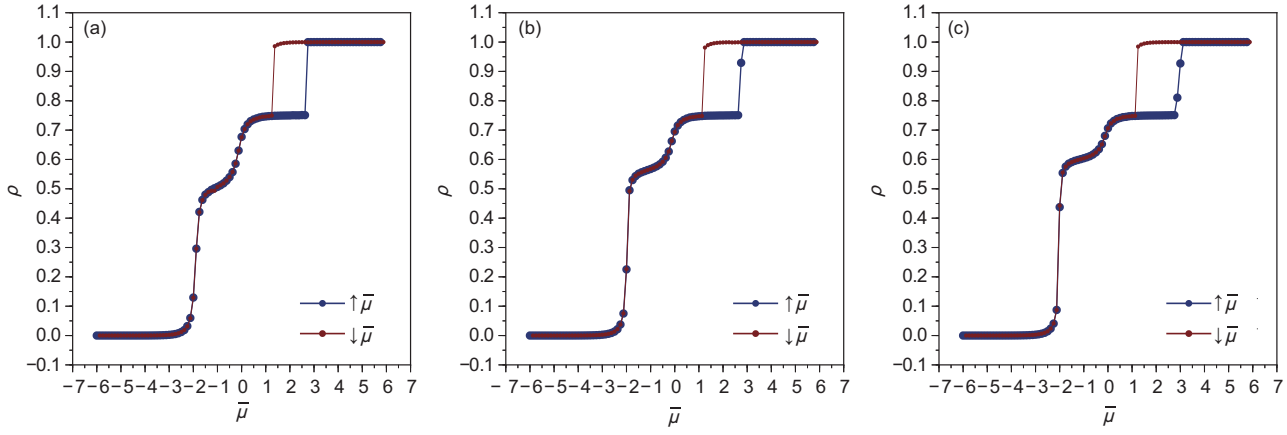

Figure 11 (Color online) Density vs. reduced chemical potential for $\overline{T}$= 0.35. (a) L_x = 6, (b) L_x = 8 and (c) L_x = 10.

Downloaded to IP: 192.168.0.24 On: 2019-05-28 09:08:46 http://engine.scichina.com/doi/10.1007/s11433-019-9416-3

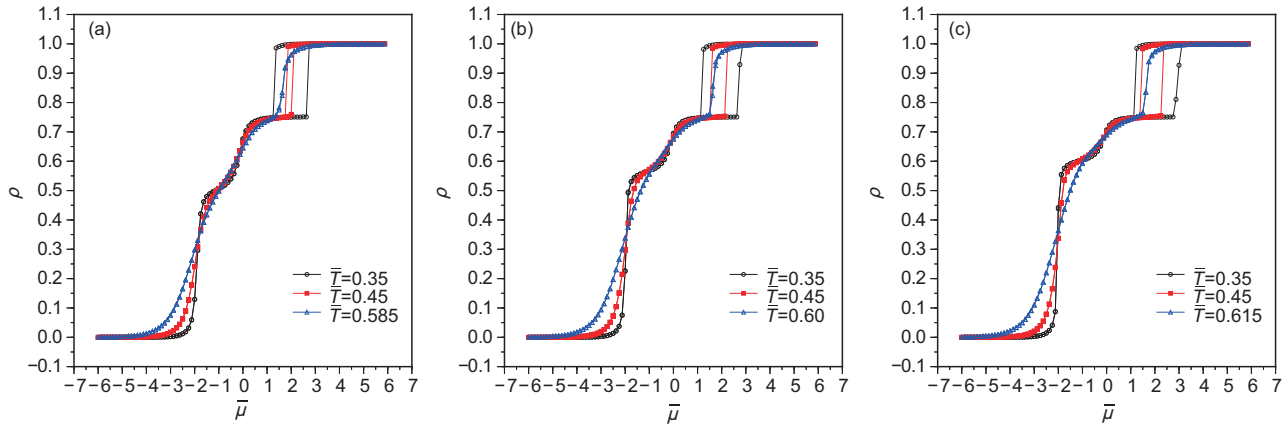

Figure 12 (Color online) Density vs. reduced chemical potential for various reduced temperatures. (a) $L_x = 6$, (b) $L_x = 8$ and (c) $L_x = 10$.

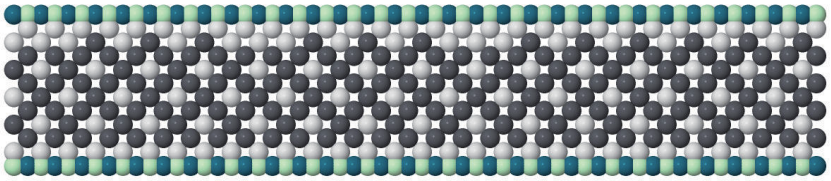

Figure 13 (Color online) Snapshot of the simulation of the confined lattice 10×30 in the *x*-*y* plane at $\overline{T}$= 0.35 and $\overline{\mu}$= 1.250.

the same for all sizes.

The LHL structure is not a result of a cooperative phenomena as expected for the drying transition [17, 21]. Even though no attraction between the wall and the fluid particles is present, the predicted transition is not present. The wall in our system acts as local reductor of the chemical potential generating a local gas phase in coexistence with a liquid phase as observed for single surfaces. One possible explanation for the absence of the transition for the system even if no attraction is present is that the arguments for the phase transition as related to depletion of water what would be consistent with a confinement in a finite system as a hydrophobic solute. In our case the system is infinite. Our result is also consistent with the behavior of large molecules and large nanotubes where no drying is observed.

In Figure 14, we present the value of the critical temperature of the LDL-HDL transition as a function of L_x. As we increase the width of the confining structure, an increase in the critical temperature of this transition is observed, approaching the value of the unconfined system as illustrated in Figure 7 [36]. However, even for separations as large as L_x=100 the bulk critical temperature is not recovered. This means that even thought the dewetting layer has an impact in the liquid-liquid critical point. This persistence of the influence of the dewetting layer on the criticality might be due to the very attractive water-water interaction we employ in our model. The gas-liquid phase transition was only observed for sizes above $L_x = 20$.

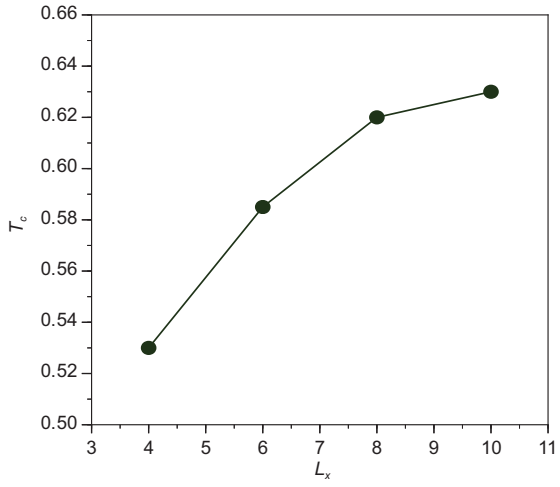

Figure 14 Critical temperature of the LDL-HDL transition as a function of L_x.

4 Conclusions

We investigated the phase behavior of the Associating Lattice Gas model confined by two hydrophobic walls.

We observed that extreme confinement suppresses phase transitions. Increasing the number of layers we noticed the emergence of the LDL-HDL transition at temperatures below those observed in the unconfined system. As the confining distance, L_x, increases the LDL-HDL critical temperature increases approaching the bulk value which is not reached since

Downloaded to IP: 192.168.0.24 On: 2019-05-28 09:08:46 http://engine.scichina.com/doi/10.1007/s11433-019-9416-3

the wetting layers affects even for large systems the criticality.

In addition a new structure, the low hydration liquid, appears. It is composed by a Low Density Liquid phase in contact with a gas layer at the wall. This new structure is present for all the sizes studied and it always have just one layer of dewetting at each wall. The confining wall works as a local lower chemical potential which is responsible for the formation of this gas layer.

The existence of the dewetting layer it is still under debate. It was observed in some confined systems [2, 20, 21, 40] but it was not found in others [41, 42]. Our assumption is that the presence of the gas-like layer is present only for very hydrophobic walls [40]. In our case water-water bond interaction is very attractive what makes the water-wall interaction very hydrophobic.

Our simple model suggests that the drying transition is not only suppressed by the addition of attractive forces but also is not present in confinement by large surfaces as the case we study.

Our analysis was only performed for the case of rigid walls. Flexibility of the walls, relevant for biological systems, might impact the layers by making them less organized [41, 43, 44], particularly close to the wall surface.

This work was supported by the Brazilian agencies CNPq, INCT-FCx, and Capes and the SECITI of Mexico city.

1 P. Ternes, E. Salcedo, and M. C. Barbosa, Phys. Rev. E **97**, 033104 (2018), arXiv: 1801.03568.
2 O. Beckstein, and M. S. P. Sansom, Proc. Natl. Acad. Sci. USA **100**, 7063 (2003).
3 E. Tajkhorshid, P. Nollert, M. Ø. Jensen, L. J. W. Miercke, J. O'Connell, R. M. Stroud, and K. Schulten, Science **296**, 525 (2002).
4 K. Murata, K. Mitsuoka, T. Hirai, T. Walz, P. Agre, J. B. Heymann, A. Engel, and Y. Fujiyoshi, Nature **407**, 599 (2000).
5 D. Fu, A. Libson, L. J. W. Miercke, C. Weitzman, P. Nollert, J. Krucinski, and R. M. Stroud, Science **290**, 481 (2000).
6 H. Sui, B. G. Han, J. K. Lee, P. Walian, and B. K. Jap, Nature **414**, 872 (2001).
7 M. R. Harpham, B. M. Ladanyi, N. E. Levinger, and K. W. Herwig, J. Chem. Phys. **121**, 7855 (2004).
8 K. Wu, Z. Chen, J. Li, X. Li, J. Xu, and X. Dong, Proc. Natl. Acad. Sci. USA **114**, 3358 (2017).
9 V. Saraswat, R. M. Jacobberger, J. S. Ostrander, C. L. Hummell, A. J. Way, J. Wang, M. T. Zanni, and M. S. Arnold, ACS Nano **12**, 7855 (2018).
10 J. K. Holt, H. G. Park, Y. Wang, M. Stadermann, A. B. Artyukhin, C. P. Grigoropoulos, A. Noy, and O. Bakajin, Science **312**, 1034 (2006).
11 M. H. Kohler, J. R. Bordin, and M. C. Barbosa, J. Mol. Liquids **277**, 516 (2019).
12 L. Liu, S. H. Chen, A. Faraone, C. W. Yen, and C. Y. Mou, Phys. Rev. Lett. **95**, 117802 (2005).
13 L. Xu, P. Kumar, S. V. Buldyrev, S. H. Chen, P. H. Poole, F. Sciortino, and H. E. Stanley, Proc. Natl. Acad. Sci. USA **102**, 16558 (2005).
14 P. Gallo, M. Rovere, and S. H. Chen, J. Phys. Chem. Lett. **1**, 729 (2010).
15 S. Cerveny, F. Mallamace, J. Swenson, M. Vogel, and L. Xu, Chem. Rev. **116**, 7608 (2016).
16 F. H. Stillinger, J Solution Chem **2**, 141 (1973).
17 K. Lum, D. Chandler, and J. D. Weeks, Int. J. Food Prop. 103, 4570 (1999).
18 T. R. Jensen, M. Østergaard Jensen, N. Reitzel, K. Balashev, G. H. Peters, K. Kjaer, and T. Bjørnholm, Phys. Rev. Lett. **90**, 086101 (2003).
19 D. Schwendel, T. Hayashi, R. Dahint, A. Pertsin, M. Grunze, R. Steitz, and F. Schreiber, Langmuir **19**, 2284 (2003).
20 Z. Zhang, S. Ryu, Y. Ahn, and J. Jang, Phys. Chem. Chem. Phys. **20**, 30492 (2018).
21 A. Wallqvistt, and B. J. Berne, J. Phys. Chem. **99**, 2893 (1995).
22 X. Huang, C. J. Margulis, and B. J. Berne, Proc. Natl. Acad. Sci. USA **100**, 11953 (2003).
23 N. Giovambattista, P. J. Rossky, and P. G. Debenedetti, Phys. Rev. E **73**, 41604 (2006).
24 N. Giovambattista, P. J. Rossky, and P. G. Debenedetti, J. Phys. Chem. B **113**, 13723 (2009).
25 P. R. ten Wolde, and D. Chandler, Proc. Natl. Acad. Sci. USA **99**, 6539 (2002).
26 P. Liu, X. Huang, R. Zhou, and B. J. Berne, Nature **437**, 159 (2005).
27 L. Hua, X. Huang, P. Liu, R. Zhou, and B. J. Berne, J. Phys. Chem. B **111**, 9069 (2007).
28 R. Zhou, X. H. Huang, C. J. Margulis, and B. J. Berne, Science **305**, 1605 (2004).
29 J. L. MacCallum, M. S. Moghaddam, H. S. Chan, and D. P. Tieleman, Proc. Natl. Acad. Sci. USA **104**, 6206 (2007).
30 G. Cicero, J. C. Grossman, E. Schwegler, F. Gygi, and G. Galli, J. Am. Chem. Soc. **130**, 1871 (2008).
31 A. Scodinu, and J. T. Fourkas, J. Phys. Chem. B **106**, 10292 (2002).
32 H. I. Kim, J. G. Kushmerick, J. E. Houston, and B. C. Bunker, Langmuir **19**, 9271 (2003).
33 B. Bagchi, Chem. Rev. **105**, 3197 (2005).
34 V. B. Henriques, and M. C. Barbosa, Phys. Rev. E **71**, 031504 (2005).
35 M. M. Szortyka, and M. C. Barbosa, Physica A **380**, 27 (2007).
36 M. M. Szortyka, V. B. Henriques, M. Girardi, and M. C. Barbosa, J. Chem. Phys. **130**, 184902 (2009), arXiv: 0902.1741.
37 P. Kumar, S. V. Buldyrev, F. W. Starr, N. Giovambattista, and H. E. Stanley, Phys. Rev. E **72**, 051503 (2005).
38 E. B. Moore, J. T. Allen, and V. Molinero, J. Phys. Chem. C **116**, 7507 (2012).
39 A. Barati Farimani, and N. R. Aluru, J. Phys. Chem. C **120**, 23763 (2016).
40 X. Li, J. Li, M. Eleftheriou, and R. Zhou, J. Am. Chem. Soc. **128**, 12439 (2006).
41 J. R. Bordin, L. B. Krott, and M. C. Barbosa, J. Phys. Chem. C **118**, 9497 (2014).
42 F. Leoni, and G. Franzese, J. Chem. Phys. **141**, 174501 (2014), arXiv: 1406.1996.
43 L. Ruiz Pestana, L. E. Felberg, and T. Head-Gordon, ACS Nano **12**, 448 (2018).
44 B. H. S. Mendonça, D. N. de Freitas, M. H. Köhler, R. J. C. Batista, M. C. Barbosa, and A. B. de Oliveira, Physica A **517**, 491 (2019), arXiv: 1803.01084.

Downloaded to IP: 192.168.0.24 On: 2019-05-28 09:08:46 http://engine.scichina.com/doi/10.1007/s11433-019-9416-3